Supplementary Information

for

Magneto-structural diverisity of Co(II) compounds of 1–benzylimidazole induced by linear pseudohalide coligands

Anna Świtlicka*[a], Barbara Machura[a], Rafał Kruszynski[b], Nicolás Moliner[c], José Miguel Carbonell[c], Joan Cano*[c], Francesc Lloret[c] and Miguel Julve[c]

[a]*Department of Crystallography, Institute of Chemistry, University of Silesia, 9th Szkolna St., 40-006 Katowice, Poland, E-mail: anna.switlicka@us.edu.pl*

[b]*Department of X-ray Crystallography and Crystal Chemistry, Institute of General and Ecological Chemistry, Lodz University of Technology, Zeromskiego St. 116, 90-924 Łodz, Poland*

[c]*Department of Química Inorgànica/Instituto de Ciencia Molecular (ICMol), Facultat de Quimica de la Universitat de València, C/ Catedrático Jose Beltrán 2,46980 Paterna, València, Spain. E-mail: miguel.julve@uv.es*

Table of contents

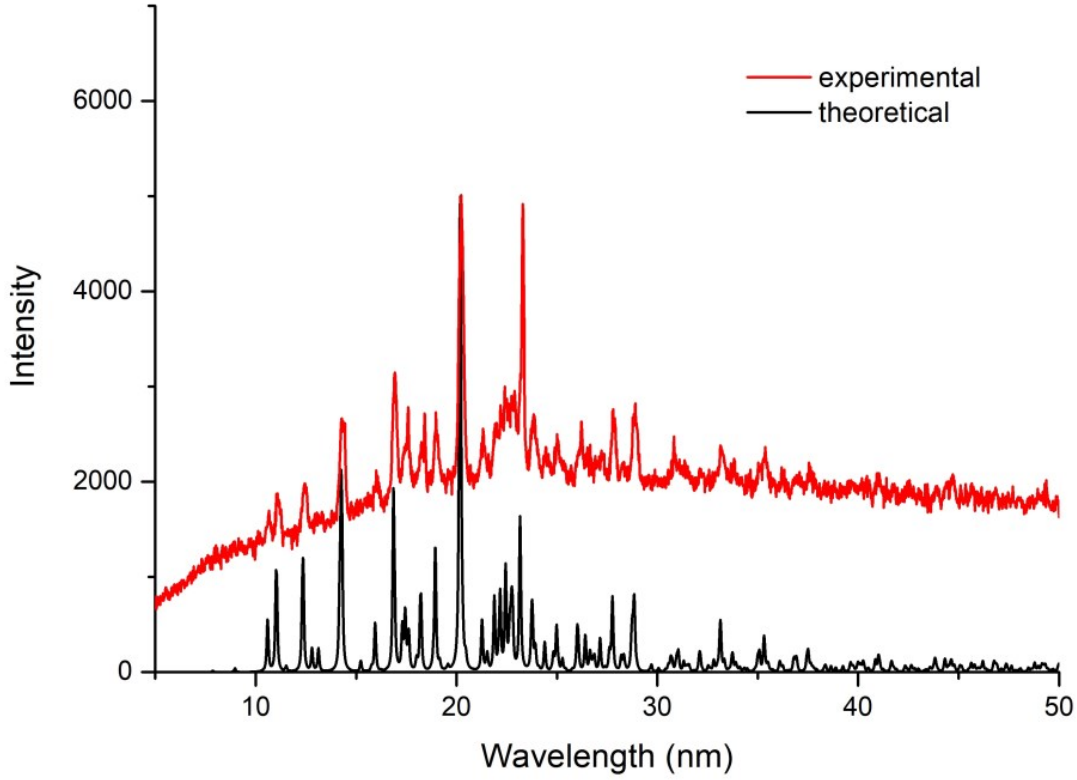

Fig. S1. XRPD pattern for **1**.

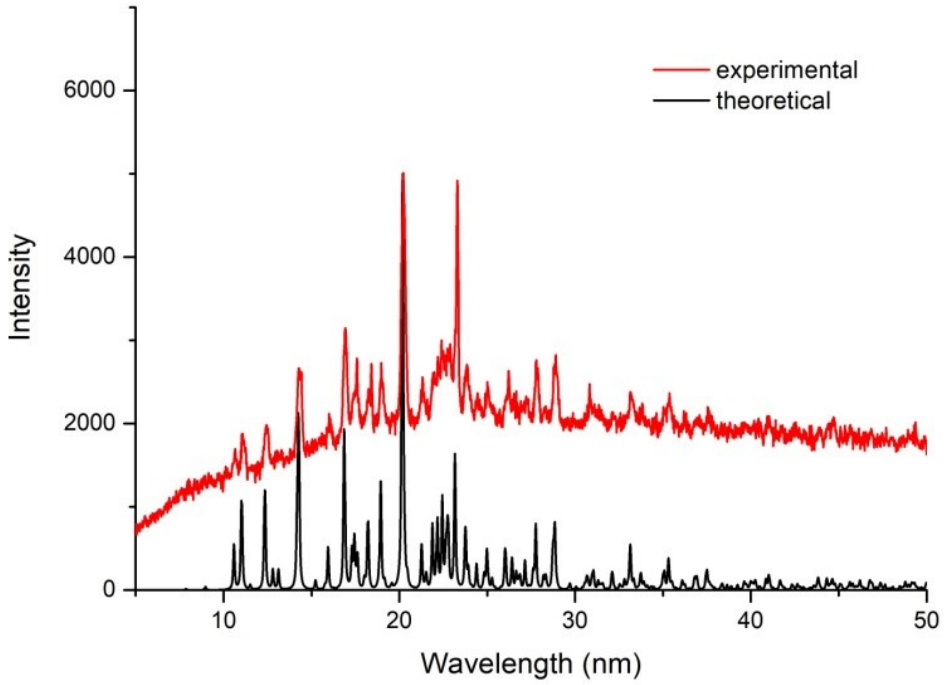

Fig.S2. XRPD pattern for **2**.

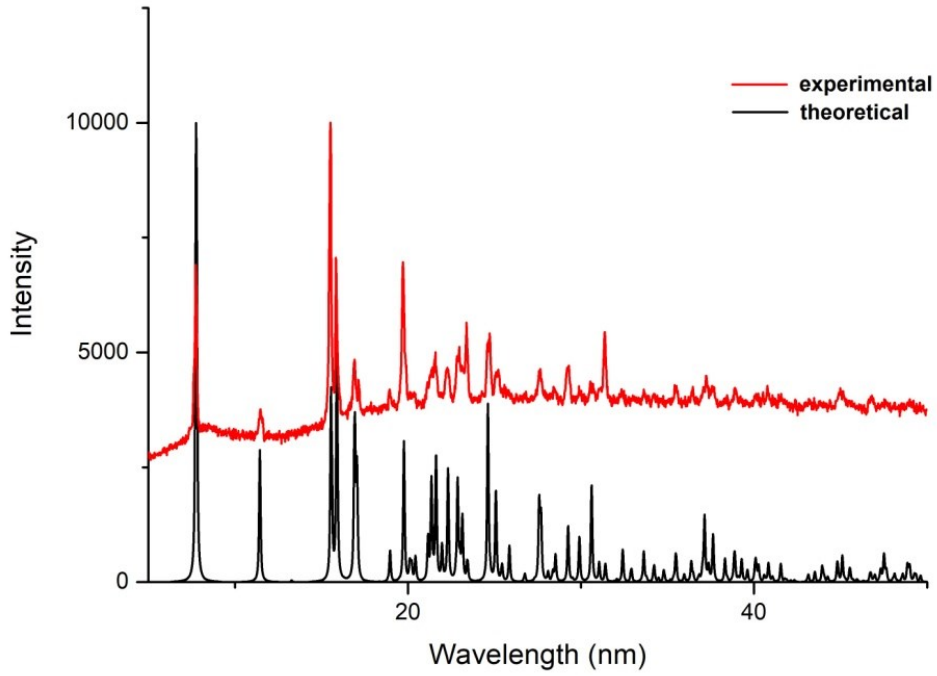

Fig. S3. XRPD pattern for **3**.

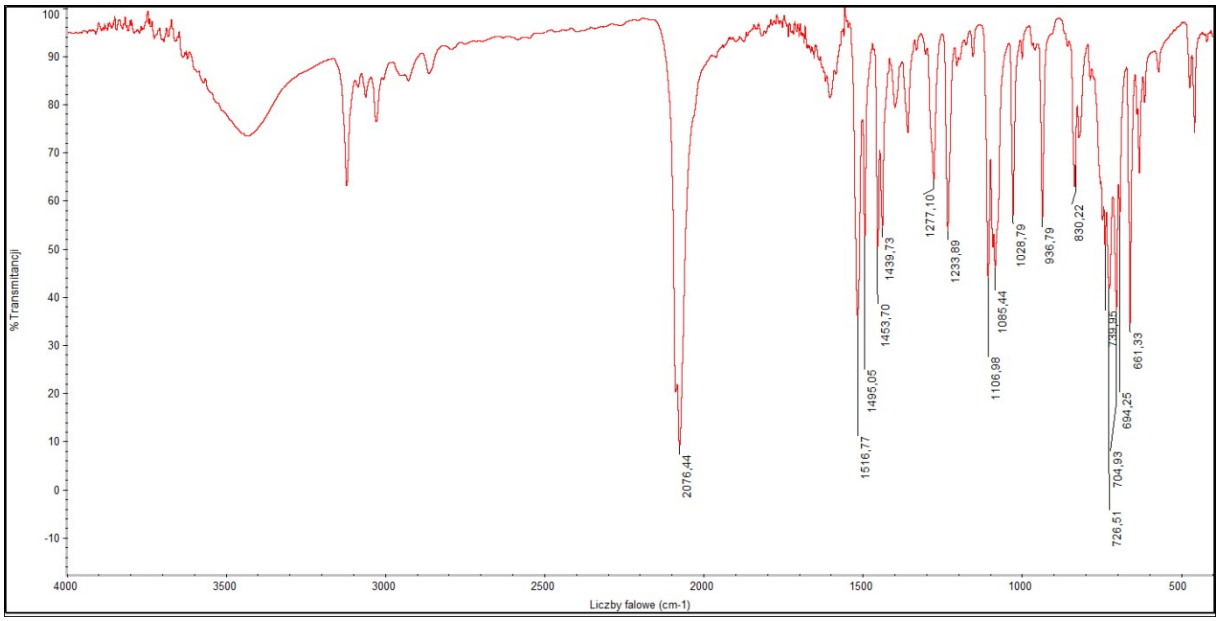

Fig. S4. IR spectrum for **1**.

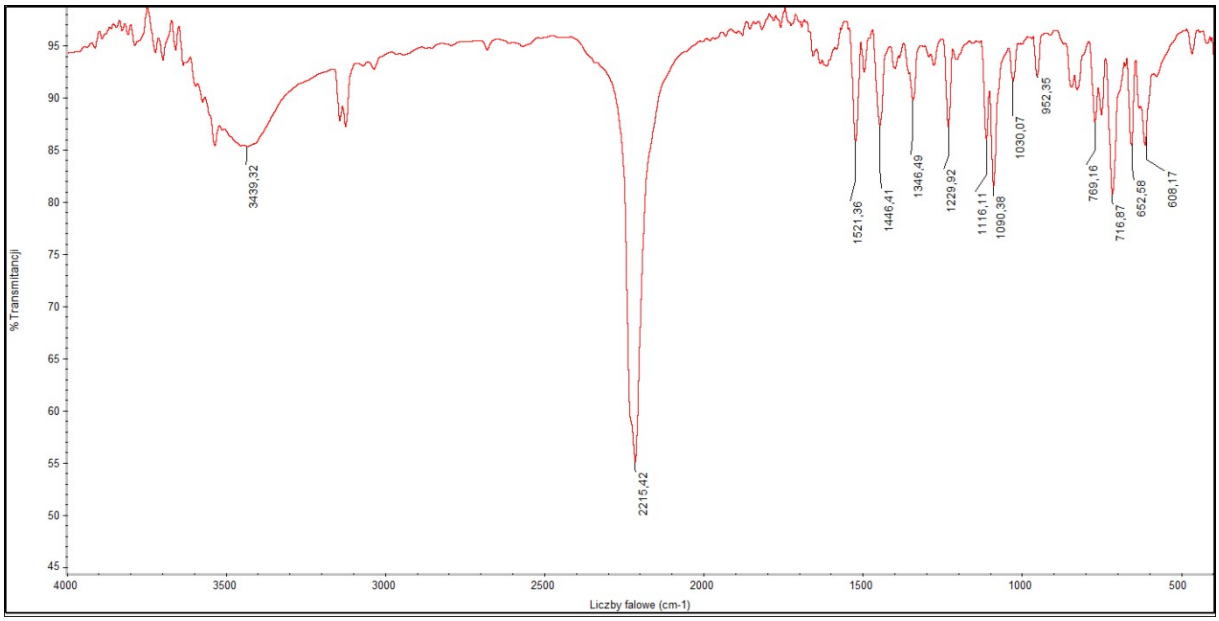

Fig. S5. IR spectrum for **2**.

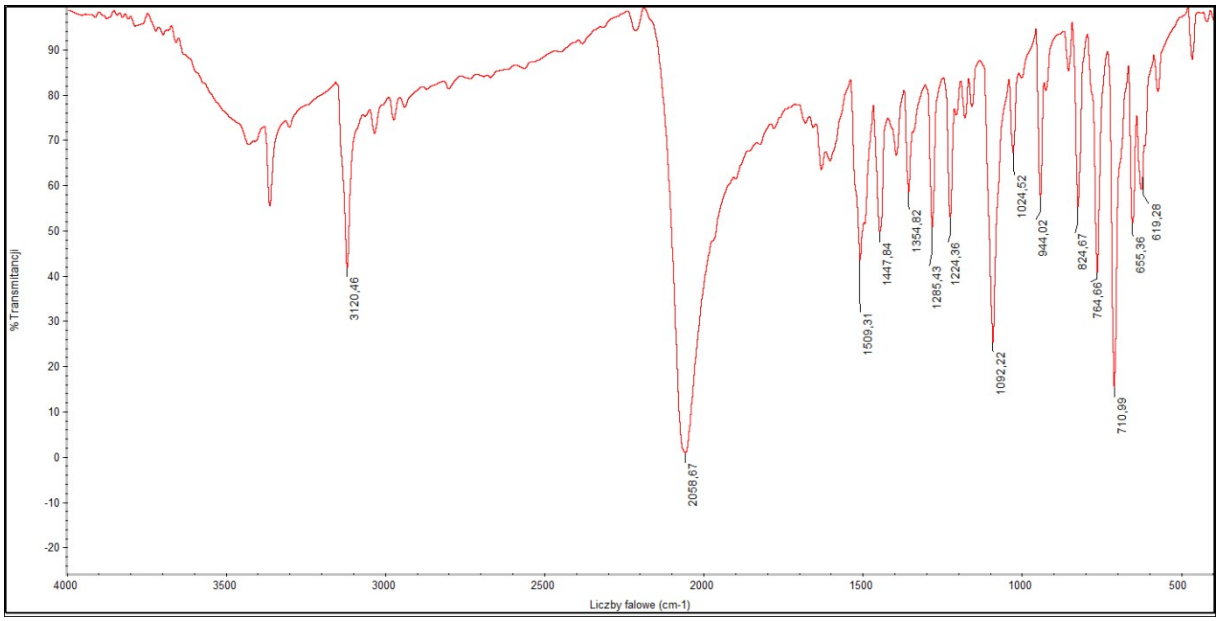

Fig. S6. IR spectrum for **3**.

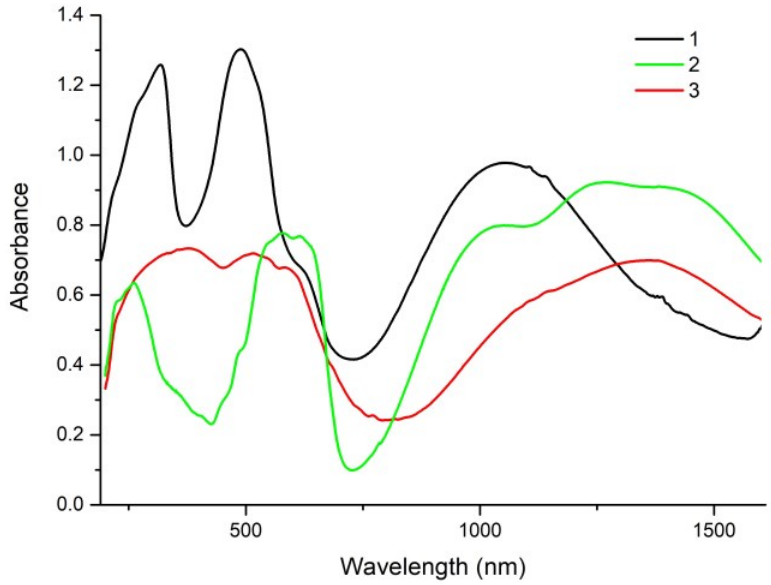

Fig. S7. UV-VIS-NIR spectra of **1**–**3**.

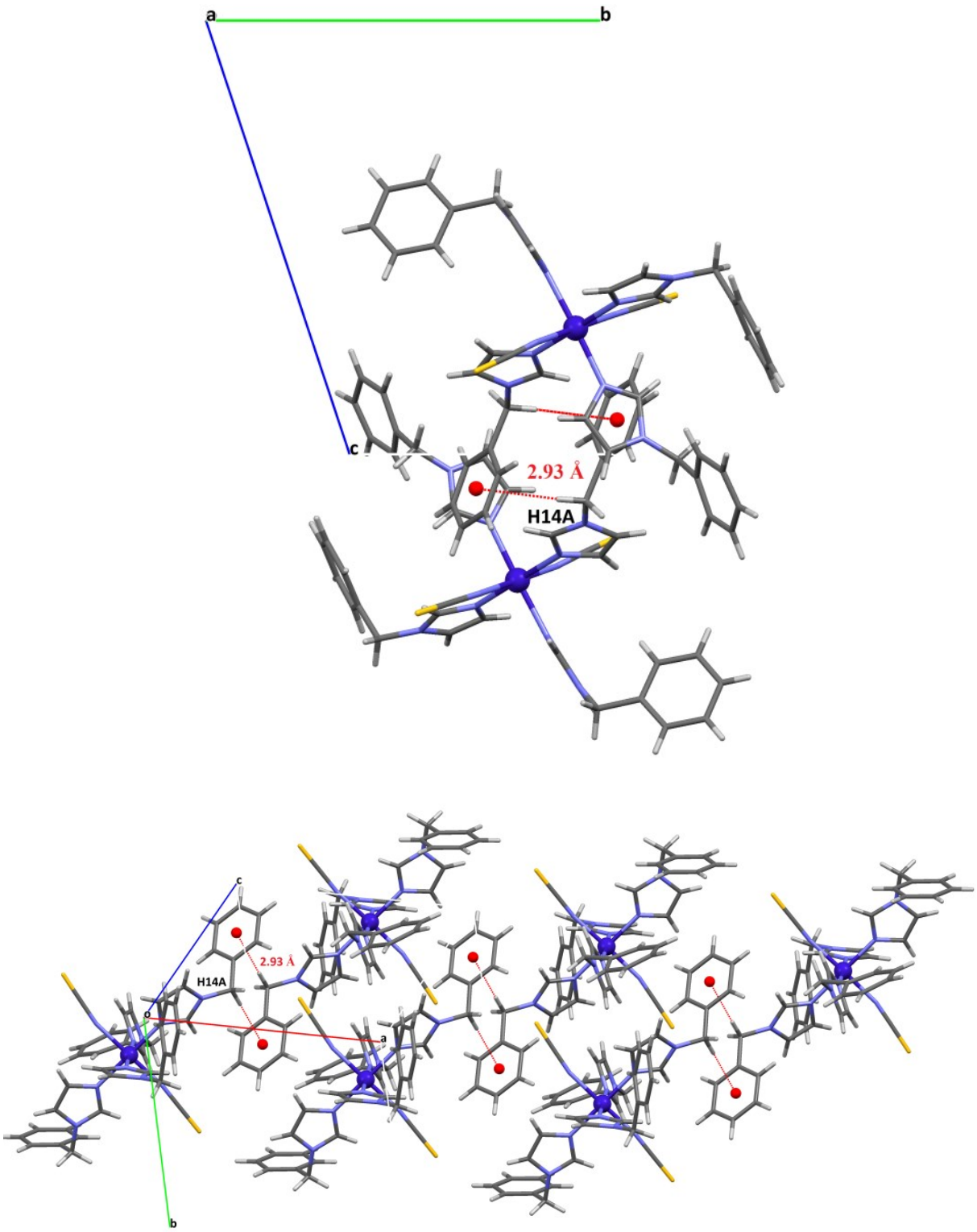

Fig. S8. A view of the crystal packing in **1** showing the intermolecular C–H•••π type interactions.

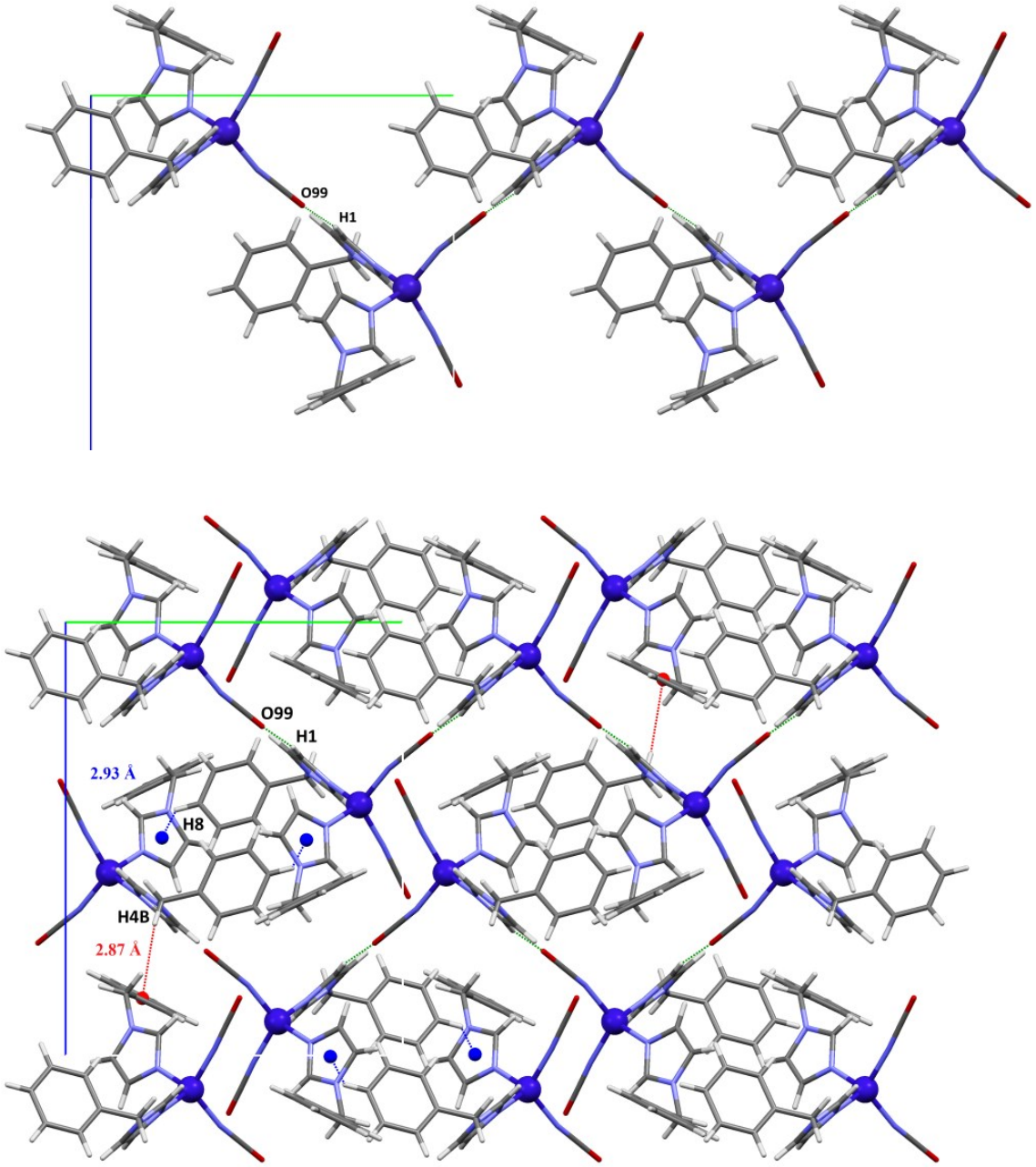

Fig. S9. A view of the packing in **2** showing the supramolecular C–H•••O and C–H•••π type interactions.

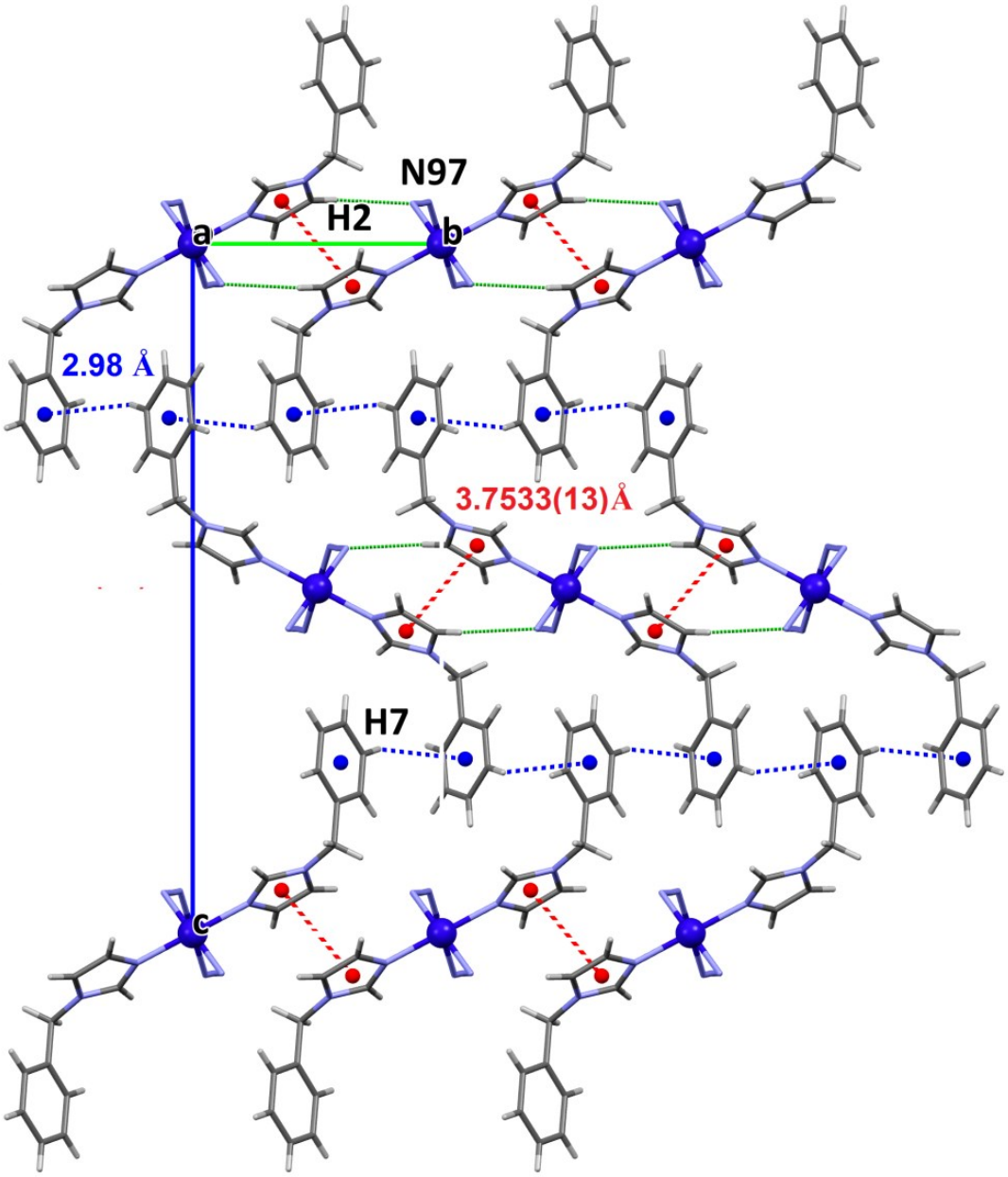

Fig. S10. A view of the supramolecular 2D network in **3** that is generated by C–H•••N, C–H•••π and π–π stacking interactions involving the bim ligands.

Table S1. Selected bond lengths [Å] and angles [°] for **1–3***

Bond lengths		Bond angles	
		1	
Co(1)–N(1)	2.134(3)	N(1)–Co(1)–N(3)	88.66(11)
Co(1)–N(3)	2.164(3)	N(1)–Co(1)–N(5)	177.62(12)
Co(1)–N(5)	2.140(3)	N(1)–Co(1)–N(7)	90.98(11)
Co(1)–N(7)	2.140(3)	N(3)–Co(1)–N(5)	88.96(12)
Co(1)–N(98)	2.111(3)	N(3)–Co(1)–N(7)	179.31(12)
Co(1)–N(99)	2.115(4)	N(5)–Co(1)–N(7)	91.39(12)
		N(98)–Co(1)–N(1)	90.88(12)
		N(98)–Co(1)–N(3)	89.81(12)
		N(98)–Co(1)–N(5)	89.13(14)
		N(98)–Co(1)–N(7)	90.79(12
		N(99)–Co(1)–N(1)	89.35(13)
		N(99)–Co(1)–N(3)	89.18(13)
		N(99)–Co(1)–N(5)	90.60(16)
		N(99)–Co(1)–N(7)	90.23(13)
		N(98)–Co(1)–N(99)	178.95(13)
		Co(1)–N(99)–C(99)	167.9(3)
		Co(1)–N(98)–C(98)	169.9(3)
		S(98)–C(98)–N(98)	179.4(4)
		S(99)–C(99)–N(99)	177.9(4)
		2	
Co(1)–N(1)	2.0192(19)	N(1)–Co(1)–N(3)	109.13(8)
Co(1)–N(3)	2.0116(19)	N(1)–Co(1)–N(98)	104.64(9)
Co(1)–N(98)	1.934(2)	N(1)–Co(1)–N(99)	110.96(8)
Co(1)–N(99)	1.928(2)	N(3)–Co(1)–N(98)	105.34(9)
		N(3)–Co(1)–N(99)	108.37(9)
		N(98)–Co(1)–N(99)	118.03(11)
		Co(1)–N(98)–C(98)	175.7(3)
		Co(1)–N(99)–C(99)	168.4(2)
		O(98)–C(98)–N(98)	178.5(3)
		O(99)–C(99)–N(99)	179.6(3)
		3	
Co(1)–N(1)	2.1181(17)	N(1)–Co(1)–N(1)a	180.0
Co(1)–N(1)a	2.1181(17)	N(1)–Co(1)–N(99)	88.90(7)
Co(1)–N(97)	2.1865(19)	N(1)a–Co(1)–N(99)	91.10(7)
Co(1)–N(97)a	2.1865(19)	N(1)–Co(1)–N(99)a	91.10(7) .
Co(1)–N(99)	2.1783(18)	N(1)a–Co(1)–N(99)a	88.90(7)
Co(1)–N(99)a	2.1783(18)	N(1)–Co(1)–N(97)a	89.85(7)
		N(1)a–Co(1)–N(97)	89.85(7)
		N(1)a–Co(1)–N(97)a	90.15(7)
		N(1)–Co(1)–N(97)	90.15(7)
		N(99)–Co(1)–N(99)a	180.0
		N(97)a–Co(1)–N(97)	180.0
		N(99)a– Co(1)– N(97)a	88.56(7)
		N(99)– Co(1)– N(97)	88.56(7)
		N(99)– Co(1)–N(97)a	88.56(7)
		N(99)–Co(1)–N(97)	91.44(7)
		N(99)a–Co(1)–N(97)	88.56(7)

Co(1)–N(99)–N(98)	137.74(15)
Co(1)–N(97)–N(98)	122.63(15)
N(97)–N(98)–N(99)	177.1(2)

*Symmetry transformations used to generate equivalent atoms: (a)= 1-*x*, *y*, 1/2-*z*.

Table S2. C–X•••Cg(J)(π–ring) (X = O, N) interactions for **1–3**

C–X(I)•••Cg(J)	X(I)•••Cg(J) [Å]	X–Perp [Å]	γ [°][b]	C–X(I)•••Cg(J) [°]
		1		
C(14)–H(14a)•••Cg(1)[b]	2.93	2.81	16.54	176
		2		
C(4)–H(4b)•••Cg(2)[c]	2.87	-2.65	22.41	165
C(8)–H(8)•••Cg(3)[d]	2.93	-2.64	25.49	121
		3		
C(7)–H(7)•••Cg(4)[e]	2.98	2.80	20.22	135

[a]Symmetry codes: (b)= 2-*x*,-*y*,-*z*; (c)= -1+*x*, 1/2-*y*, 1/2+*z*; (d)= 1-*x*,-*y*,-*z*; (e)= 1/2-*x*,-1/2+*y*,1/2-*z*

[b] γ = angle X(I)→Cg(J) vector and normal to plane J.

[c] Cg(1) is the centroid of the C(15)/C(16)/C(17)/C(18)/C(19)/C(20) set of atoms.
Cg(2) is the centroid of the /C(15)/ C(16)/C(17)/C(18)/C(19)/C(20) set of atoms.
Cg(3) is the centroid of the N(3)/C(11)/ C(12)/N(4)/C(13) set of atoms.
Cg(4) is the centroids of the C(5)/C(6)/C(7)/C(8)/C(9)/C(10) set of atoms.

Table S3. Short intra– and intermolecular contacts in **2** and **3***

D—H•••A	D—H	H•••A	D•••A [Å]	D—H•••A [°]
		2		
C(1)–H(1)•••O(99)[f]	0.93	2.41	3.331(3)	171.0
		3		
C(2)–H(2)•••N(97)[g]	0.93	2.57	3.379(3)	145.0
C(3)–H(3)•••N(99)	0.93	2.58	3.085(3)	114.0

*Symmetry transformations used to generate equivalent atoms: (f) = 2-*x*,-1/2+*y*,1/2-*z*; (g) = *x*,-1+*y*, *z*.

Table S4. Short π•••π stacking interactions in **3***,[&]

Cg(I)•••Cg(J)	Cg(I)•••Cg(J) [Å]	α [°]	β [°]	γ [°]	Cg(I)-Perp [Å]	Cg(J)-Perp [Å]
			3			
Cg(5)•••Cg(5)[h]	3.7533(13)	0	24.04	24.04	-3.4277(9)	-3.4277(9)

*α = dihedral angle between *Cg*(I) and *Cg*(J); *Cg*(I)-Perp = Perpendicular distance of *Cg*(I) on ring J; *Cg*(J)-Perp = perpendicular distance of *Cg*(J) on ring I; β = angle *Cg*(I)→*Cg*(J) vector and normal to ring I; γ = angle *Cg*(I) →*Cg*(J) vector and normal to plane J; Cg(5): N(1)/C(1)/C(2)/N(2)/C(3). [&]Symmetry code: (h) = 1-*x*,-1-*y*,-*z*

Table S5. Selected magneto-structural parameters of cobalt(II) chains generated through double azido bridges*

Complex	Co–N_L [Å]	Co– $\mu_{1,3}N_3$ [Å]	Co–$\mu_{1,1}N_3$ [Å]	Co…Co [Å]	Co–N–N–N [°]	Co–N_3–Co [°]	Magnetic properties	Ref
double $\mu_{1,3}$–N_3								
$[Co(L^1)_2(\mu_{1,3}\text{-}N_3)_2]_n$	2.139(3) 2.140(3)	2.136(3) 2.138(3) 2.154(3) 2.161(3)	–	9.090(1)	120.6(2) 127.0(2)	–	C = 4.9 cm^3 K mol^{-1} Θ = –228 K. antiferromagntic coupling	1
$[Co(N_3)_2(L^2)_2]_n$	2.131(2) 2.135(2)	2.134(3) 2.148(3)	–	5.265(2)	129.0(2) 134.6(2)	–	J = −31.76 cm^{-1} antiferromagnetic interactions along the chains	2
double $\mu_{1,3}$–N_3 and $\mu_{1,1}$–N_3								
$[Co_{1.5}(L^3)_3(N_3)_3]_n$	2.142(3) 2.163(3) 2.148(3) 2.148(3)	2.181(3) 2.165(3)	2.141(3) 2.144(3)	$\mu_{1,1}$–N_3 3.307(4) $\mu_{1,3}$–N_3 5.038(1)	125.2(2) 121.8(3)	100.7 100.9	C = 10.01 cm^3 mol^{-1} K Θ = 229.02 K J_t = 12.36 cm^{-1}, J_c = 24.06 cm^{-1} antiferromagnetic interactions	3
$[Co_2(\mu_{1,1}\text{-}N_3)_2(\mu_{1,3}\text{-}N_3)_2(L^4)_4]_n$	2.158(2) 2.132(2) 2.141(2) 2.158(2)	2.149(2) 2.155(2) 2.181(2) 2.161(2)	2.144(2) 2.143(2) 2.146(2) 2.137(2)	$\mu_{1,1}$–N_3 3.2803(4) $\mu_{1,3}$–N_3 4.9922(4)	123.23(19) 127.22(18) 117.61(17)	99.84(9), 100.00(9)	C = 3.70 cm^3 mol^{-1} K Θ = –65.9 K.	4
$[Co_3(\mu_{1,1}\text{-}N_3)_4(\mu_{1,3}\text{-}N_3)_2(L^5)_6]_n$	2.1568(11) 2.1568(11) 2.1900(11) 2.1439(11)	2.1436(11) 2.1436(11) 2.1302(12) 2.1302(12)	2.1438(10) 2.11198(11) 2.1230(11) 2.1636(11)	$\mu_{1,1}$–N_3 3.2356(3) $\mu_{1,3}$–N_3 4.9280(4)	123.56(9) 120.91(9)	98.73(4) 98.01(4)	C = 3.9 cm^3 mol^{-1} K Θ = –63.6 K.	4

$[Co(L^6)(N_3)_2]_n$	2.125(2) 2.119(2)	2.189(3) 2.133(3)	2.128(2) 2.180(3)	$\mu_{1,1}$–N_3 3.323(2) $\mu_{1,3}$–N_3 5.279(2)	129.9(2) 127.1(2)	100.94(9)	metamagnetic-like behaviour	5
$[Co(L^7)(N_3)_2]_n$	2.1305(17) 2.1128(18)	2.1599(18) 2.1712(19) 2.163(2) 2.163(2)	2.130(2) 2.130(2)	$\mu_{1,1}$–N_3 3.407 $\mu_{1,3}$–N_3 5.366	126.69(15) 128.34(15)	103.70(8)	weak ferromagnetic behavior due to the spin-canting (spin-canting behavior should be attributed to the single-ion anisotropy of Co(II) ions)	6
$[Co_2(L^8)_2(N_3)_4]_n$	1.978(3)	2.408(4) 1.978(4)	2.021(3) 1.994(3)	$\mu_{1,1}$–N_3 3.09 3.26 $\mu_{1,3}$–N_3 5.12	116.9(3) 131.2(3)	100.26 94.76	U_{eff} = 22.46 K (16.25cm^{-1}) τ_0 =3.31·10^{-8} s	7
$[Co_2(N_3)_4(L^9)_4]_n$	2.170(5) 2.150(5)	2.168(6) 2.154(5)	2.137(5) 2.135(5)	$\mu_{1,1}$–N_3 3.282 $\mu_{1,3}$–N_3 4.965	121.4(5) 121.8(4) 122.1(4) 124.6(5)	100.6(3) 100.8(2)	J_1 =25.16 cm^{-1}, J_2 = −38.30 cm^{-1}, antiferromagnetic coupling	2
double $\mu_{1,1}$–N_3								
$[Co(L^{10})(N_3)_2]_n$	2.155(4) 2.148(4) 2.164(4) 2.171(4) 2.128(3) 2.163(4)	–	2.102(5) 2.132(6) 2.112(5) 2.131(6) 2.151(7) 2.125(6)	3.334(1) 3.344(1) 3.636(2)	–	102.9(2) 116.0(4)	*C* =3.095(8)cm^3mol^{-1} K Θ= +35.9(2) K *J* = 12.4(1) cm^{-1} ferromagnetic coupling in the chain	8

	2.140(6) 2.124(5)	$\tau_0 = 3.4 \cdot 10^{-12}$ s single chain magnet

*Abbreviations: L^1 = 3,5-lutidine ; L^2 = 4-benzylpyridine; L^3 = 3,5-dimethylpyridine; L^4 = 4-ethylpyridine; L^5 = 3-picoline, L^6 = 2,2,'bipyridine; L^7 = 2,2'-dipyridylamine; L^8 =1-((2-propyl-imidazol-1-yl)methyl)-benzo[1,2,3]triazole; L^9 = 4–vinylpyridine; L^{10} = 2,2'-bithiazoline.

References:

1. A. Escuer, F. A. Mautner, B. Sodin, M. A. S. Goher and R. Vicente, Topologic ferrimagnetism in cobalt(II)-azido chains, *Dalton Trans.,* 2010, **39**, 4482–4484.

2 J.-P. Zhao, C. Zhao, W.-C. Song, L. Wang, Y. Xie, J.-R. Li and X.-H. Bu, 4-Substituent pyridine directed cobalt(II) azides: solvothermal synthesis, structure, and magnetic properties, *Dalton Trans*., 2015, **44**, 10289–10296.

3. Z. Lu, P. Gamez, H. Z. Kou, C. Fan, H. Zhang and G. Sun, Spin canting and metamagnetism in the two azido-bridged 1D complexes $[Ni(3,5\text{-}dmpy)_2(N_3)_2]_n$ and $[Co_{1.5}(3,5\text{-}dmpy)_3(N_3)_3]_n$, *CrystEngComm*, 2012, **14**, 5035–5041.

4. F. A. Mautner, B. Sudy, C. Berger, R. C. Fischer and R. Vicente, Synthesis, structural and magnetic study of two new alternating 1D azido-bridged cobalt(II) complexes, *Polyhedron*, 2012, **42**, 95–101.

5. G. Viau, M. G. Lombardi, G. De Munno, M. Julve, F. Lloret, J. Faus, A. Caneschi and J. M. Clemente-Juan, The azido ligand: a useful tool in designing chain compounds exhibiting alternating ferro- and antiferro-magnetic interactions, *Chem. Commun*., 1997, 1195–1196.

6. X. T. Wang, X.-H. Wang, Z.-M. Wang and S. Gao, Diversity of Azido Magnetic Chains Constructed with Flexible Ligand 2,2′-Dipyridylamine, *Inorg. Chem.,* 2009, **48**, 1301–1308.

7. X. Ma, Y. Liu, W. Song, Z. Wang, X. Liu, G. Xie, S. Chen and S. Gao, A difunctional azido-cobalt(II) coordination polymer exhibiting slow magnetic relaxation behaviour and high-energy characteristics with good thermostability and insensitivity, *Dalton Trans.,* 2018, **47**, 12092–12104.

8. T. F. Liu, D. Fu, S. Gao, Y. Z. Zhang, H. L. Sun, G. Su and Y. J. Liu, An Azide-Bridged Homospin Single-Chain Magnet: $[Co(2,2'\text{-}bithiazoline)(N_3)_2]_n$, *J. Am. Chem. Soc*., 2003, **125**, 13976–13977.

Table S6. Energy of the calculated quartet (Q_i) and triplet (D_i) excited states and their contributions to the D and E values for **1** obtained from CASSCF/NEVPT2 calculations. D_{SS} is the spin-spin contribution to axial *zfs* parameter, and D_Q and D_D are the sum of spin-orbit contributions coming from quartet and doublet excited states

State	Energy[a]	S	D[a]	E[a]	State	Energy[a]	S	D[a]	E[a]
D_{SS}		4	+0.000	+0.000	D_5	19469.2	2	–1.098	+1.082
D_Q		4	+83.904	+9.405	D_6	19580.8	2	–0.024	+0.003
D_D		2	–3.434	–4.099	D_7	19600.7	2	–0.124	+0.095
Q_1	339.6	4	+52.131	+52.124	D_8	19624.6	2	+0.025	–0.002
Q_2	596.2	4	+38.836	–38.826	D_9	22980.1	2	+2.857	–0.000
Q_3	9893.6	4	–11.839	+0.189	D_{10}	22987.9	2	–0.056	+0.023
Q_4	9991.3	4	+4.210	–3.847	D_{11}	23056.6	2	–0.043	–0.011
Q_5	10197.5	4	+0.389	–0.238	D_{12}	27194.2	2	–0.012	–0.007
Q_6	20916.1	4	+0.001	+0.000	D_{13}	29850.2	2	+0.126	+0.152
Q_7	23411.9	4	+0.037	–0.035	D_{14}	30020.4	2	+0.243	+0.071
Q_8	23657.5	4	+0.064	–0.024	D_{15}	30298.8	2	+0.020	–0.003
Q_9	23676.0	4	+0.075	+0.062	D_{16}	31876.2	2	–0.407	–0.112
D_1	9779.3	2	+0.762	–1.173	D_{17}	31930.4	2	–0.322	+0.056
D_2	10108.8	2	–3.609	–2.417	D_{18}	32029.3	2	–0.026	–0.008
D_3	19277.4	2	–0.011	+0.010	D_{19}	33354.1	2	–0.138	–0.502
D_4	19285.7	2	–1.223	–1.203	D_{20}	33372.4	2	–0.374	–0.153

[a]Values in cm^{-1}.

Table S7. Energy of the calculated quartet (Q_i) and triplet (D_i) excited states and their contributions to the *D* and *E* values for **2** obtained from CASSCF/NEVPT2 calculations. D_{SS} is the spin-spin contribution to axial *zfs* parameter, and D_Q and D_D are the sum of spin-orbit contributions coming from quartet and doublet excited states

State	Energy[a]	*S*	*D*[a]	*E*[a]	State	Energy[a]	*S*	*D*[a]	*E*[a]
D_{SS}		4	+0.000	+0.000	D_5	20178.1	2	–0.013	–0.008
D_Q		4	–8.646	–0.081	D_6	21798.4	2	–0.001	+0.001
D_D		2	–1.185	+0.115	D_7	22939.9	2	–1.177	+1.101
Q_1	4794.9	4	–11.072	–2.547	D_8	23258.2	2	+0.857	+1.004
Q_2	4986.4	4	–4.693	–6.001	D_9	23942.9	2	–1.181	–2.002
Q_3	6159.7	4	+7.317	+7.819	D_{10}	24523.0	2	+0.632	–0.021
Q_4	8128.8	4	–0.200	+0.133	D_{11}	25769.3	2	–0.073	+0.152
Q_5	8933.4	4	–0.001	–0.023	D_{12}	26805.5	2	–0.034	+0.039
Q_6	11286.9	4	+0.006	–0.006	D_{13}	26806.7	2	+0.215	–0.039
Q_7	19565.8	4	+0.000	–0.000	D_{14}	26918.3	2	–0.023	+0.002
Q_8	22224.6	4	+0.000	–0.000	D_{15}	27401.5	2	–0.019	+0.005
Q_9	22358.4	4	–0.003	+0.000	D_{16}	27450.4	2	–0.154	–0.126
D_1	18441.8	2	–0.578	+0.544	D_{17}	28744.0	2	–0.009	+0.001
D_2	19251.6	2	–0.024	+0.019	D_{18}	28895.1	2	+0.029	–0.028
D_3	19304.1	2	–0.065	–0.067	D_{19}	29765.8	2	–0.051	+0.037
D_4	19951.7	2	–0.073	+0.030	D_{20}	29918.3	2	–0.021	+0.015

[a]Values in cm^{-1}.

Table S8. Selected ac magnetic data at different applied dc fields through Raman (R) plus temperature non-dependent intra-Kramer (IK), Thermally Activated (TA) plus IK, and two TA plus IK processes for **1**.

H_{dc}	Model	C[a]	N	τ_{01}[b] x 10^7	E_{a1}[c]	τ_{02}[b] x 10^9	E_{a2}[c]	τ_{0IK}[b] x 10^3
1000	R + IK	0.065 ± 0.017	7.09 ± 0.16					3.95 ± 0.21
	TA + IK			1.45 ± 0.11	24.2 ± 0.3			3.37 ± 0.09
	TA + TA + IK			1.04 ± 0.13	25.6 ± 0.5	2.4 ± 0.3	50.2 ± 1.1	3.48 ± 0.05
2500	R + IK	0.046 ± 0.011	7.24 ± 0.15					2.27 ± 0.07
	TA + IK			1.35 ± 0.10	24.8 ± 0.3			2.04 ± 0.04
	TA + TA + IK			3.3 ± 0.5	22.2 ± 0.5	5.1 ± 0.7	45.3 ± 1.2	2.11 ± 0.03
5000	R + IK	0.047 ± 0.014	7.22 ± 0.18					0.428 ± 0.008
	TA + IK			0.97 ± 0.05	26.25 ± 0.22			0.413 ± 0.025
	TA + TA + IK			1.5 ± 0.4	24.9 ± 0.8	4.8 ± 1.6	48 ± 3	0.415 ± 0.004

[a] Values in $s^{-1} K^{-n}$. [b] Values in s. [c] Values in cm^{-1}.

Table S9. Selected ac magnetic data at different applied dc fields through Direct (D, $\tau^{-1} = AT$) plus thermally activated Orbach (O, $\tau^{-1} = \tau_0^{-1} e^{-E_a/kT}$) or two-phonon Raman (R, $\tau^{-1} = CT^n$) mechanisms for the high- (*ht*) and low-temperature (*lt*) relaxation processes of **2**.

H_{dc}	Model	A[a]	C[b]	n	τ_0[c]	E_a[d]
			ht process			
1000	D+O	107 ± 24			(2.5 ± 1.1) x 10^{-10}	27.2 ± 1.1
	D+R	50 ± 22	0.035 ± 0.016	11.2 ± 0.3		
2500	D+O	105 ± 20			(4.9 ± 1.7) x 10^{-10}	26.4 ± 0.9
	D+R	50 ± 30	0.06 ± 0.03	10.5 ± 0.4		
5000	D+O	2180 ± 180			(7.7 ± 1.5) x 10^{-10}	25.9 ± 0.6
	D+R	1090 ± 90	0.58 ± 0.07	8.80 ± 0.08		
			lt process			
1000	O				(2.8 ± 1.2) x 10^{-8}	13.1 ± 0.7
2500	O				(10.0 ± 1.5) x 10^{-8}	11.50 ± 0.24
5000	O				-----	-----

[a] Values in $s^{-1} K^{-1}$. [b] Values in $s^{-1} K^{-n}$. [d] Values in s. [e] Values in cm^{-1}.

Table S10. Selected ac magnetic data at different applied dc fields through Direct (D, $\tau^{-1} = AT$) plus thermally activated Orbach (O, $\tau^{-1} = \tau_0^{-1} e^{-E_a/kT}$) or two-phonon Raman (R, $\tau^{-1} = CT^n$) mechanisms for the high- (*ht*) and low-temperature (*lt*) relaxation processes of **2**. *H*t and *lt* processes were individually analysed through a previous selection of the experimental data.

H_{dc}	Model	A[a]	C[b]	n	τ_0[c]	E_a[d]
			ht process			
1000	D+O	-----			(8.7 ± 0.7) x 10^{-10}	24.22 ± 0.19
	D+R	-----	0.057 ± 0.023	10.8 ± 0.3		
2500	D+O	220 ± 30			(7.5 ± 2.0) x 10^{-10}	25.4 ± 0.7
	D+R	80 ± 18	0.093 ± 0.015	10.26 ± 0.12		
5000	D+O	1840 ± 110			(3.6 ± 1.0) x 10^{-10}	27.5 ± 0.8
	D+R	1590 ± 40	0.126 ± 0.015	9.98 ± 0.09		
			lt process			
1000	O				(3 ± 4) x 10^{-7}	11.7 ± 2.0
2500	O				(19.9 ± 1.3) x 10^{-7}	8.00 ± 0.11
5000	O				-----	-----

[a] Values in $s^{-1} K^{-1}$. [b] Values in $s^{-1} K^{-n}$. [c] Values in s. [d] Values in cm^{-1}.

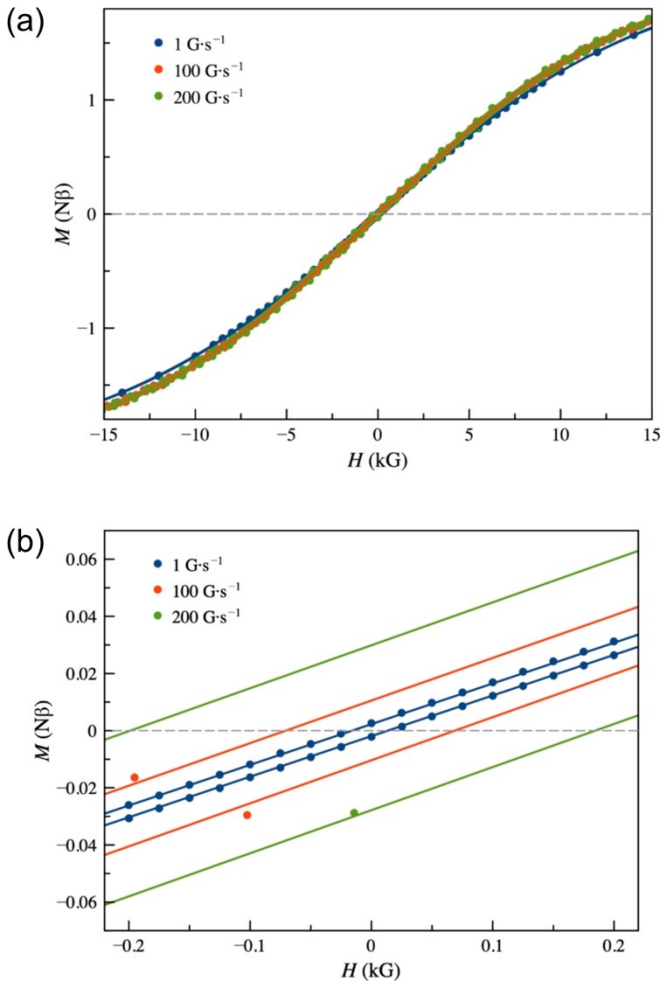

Fig. S11. (a) Hysteresis loops of **1** at 2.0 K with sweep rates of **1** (blue), 100 (red), and 200 (green) G s^{-1}. (b) A zoom of the above curve to facilitate the evaluation of the coercive magnetic field.

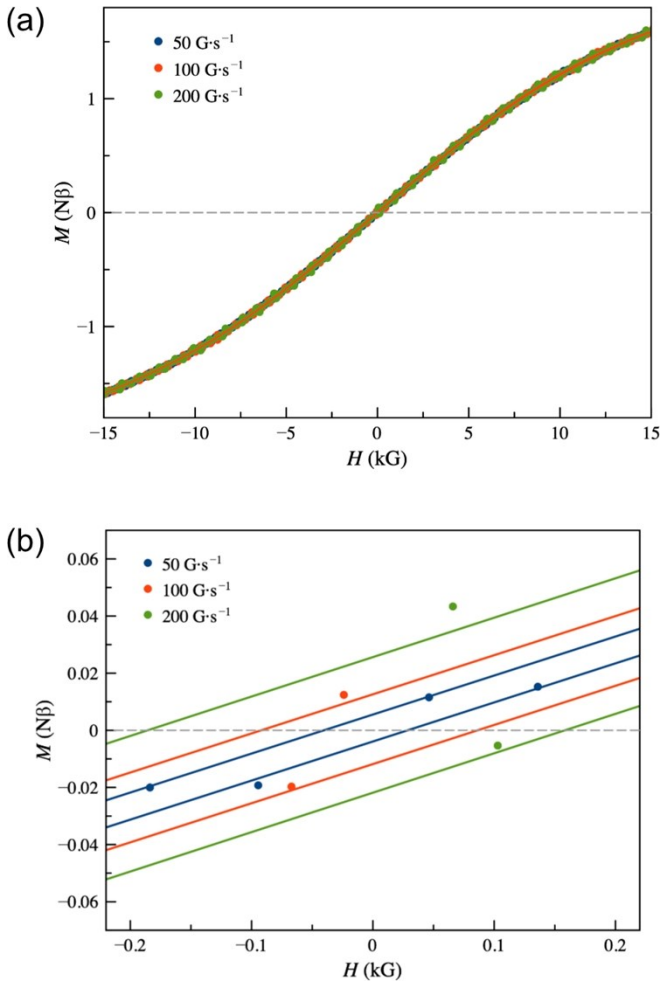

Fig. S12. (a) Hysteresis loops of **2** at 2.0 K with sweep rates of 50 (blue), 100 (red), and 200 (green) G s^{-1}. (b) A zoom of the above curve to facilitate the evaluation of the coercive magnetic field.

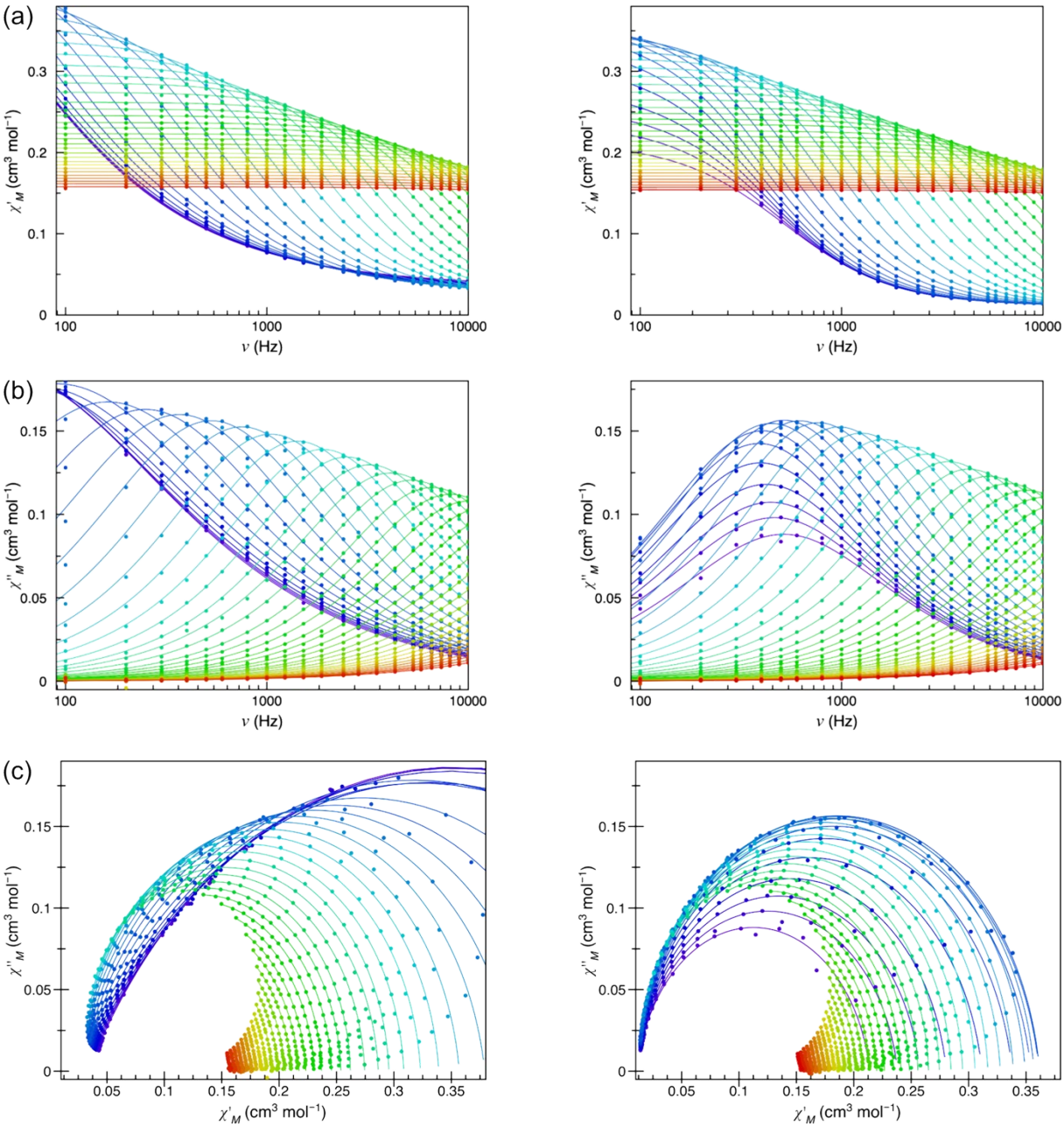

Fig. S13. Frequency dependence of χ_M' (a), χ_M" (b) and Cole-Cole plots (c) of **1** in an applied static fields H_{dc} = 1.0 (left) and 5.0 kG (right) and under ±5.0 G oscillating field at temperatures in the range 2.0-12 K in steps of 0.25 K (from blue to red). The solid lines are the best-fit curves simulated by using the general Debye model.

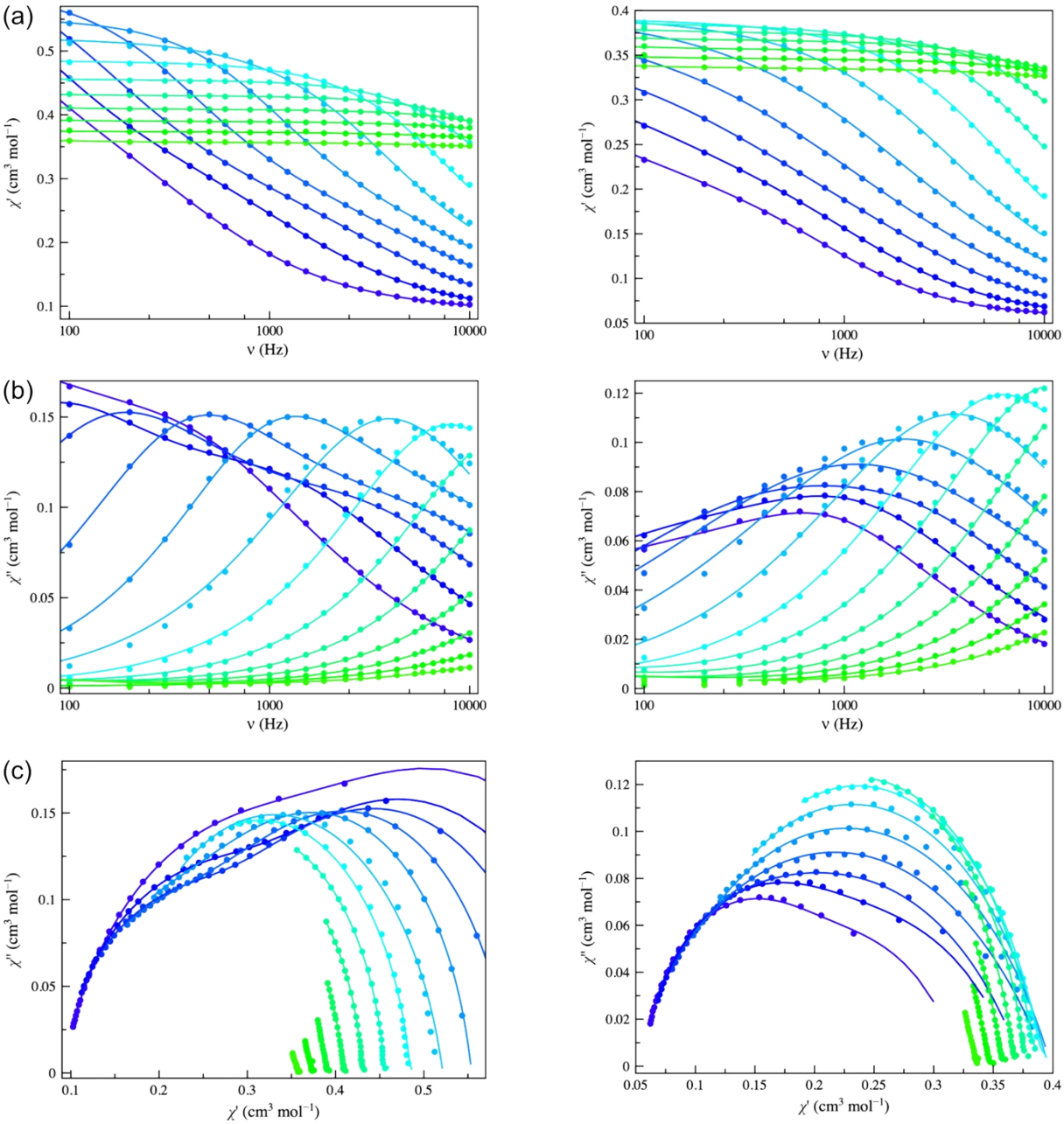

Fig. S14. Frequency dependence of χ_M' (a), χ_M" (b) and Cole-Cole plots (c) of **2** in an applied static fields H_{dc} = 1.0 (left) and 5.0 kG (right) and under ±5.0 G oscillating field at temperatures in the range 2.0-5.0 K in steps of 0.25 K (from blue to red). The solid lines are the best-fit curves simulated by using the general Debye model.

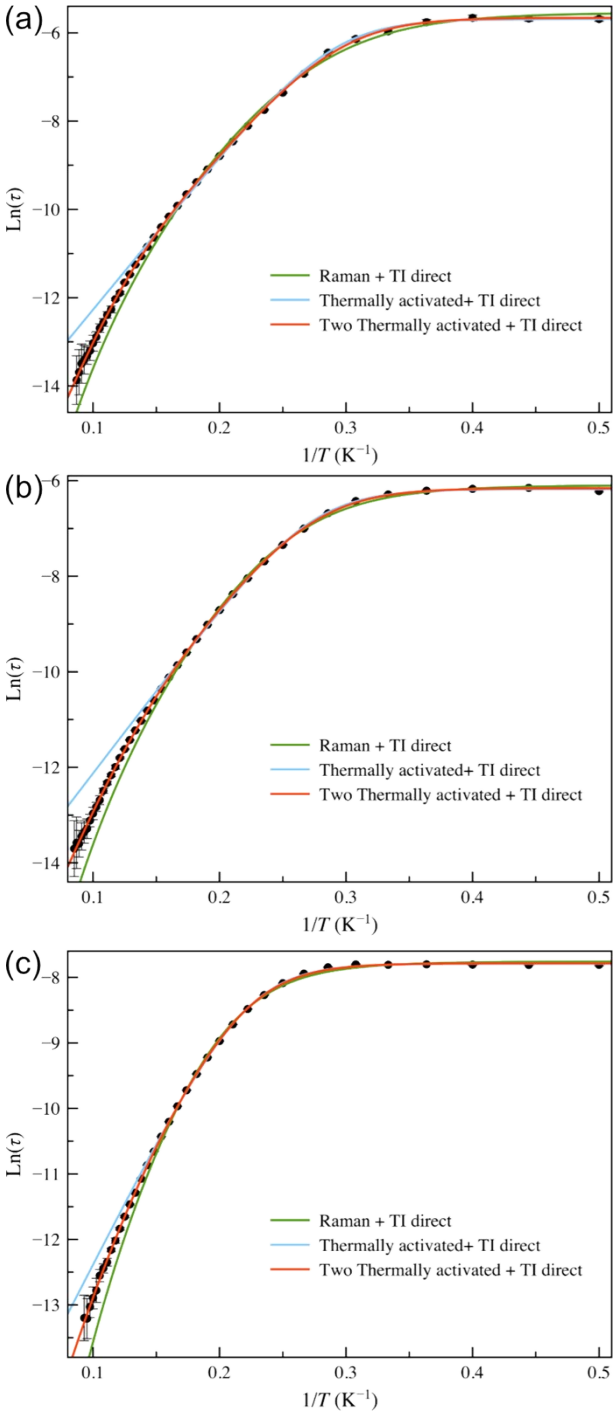

Fig. S15. Arrhenius plots (●) for **1** under applied dc fields of (a) 1000, (b) 2500 and (c) 5000 G. The solid lines are the best-fit curves according to the Raman + IK and Orbach + IK models in the temperature range 2.0-6.0 K) and to the double Orbach + IK combination in the temperature range 2.0-11.75 K (see details in the main text).

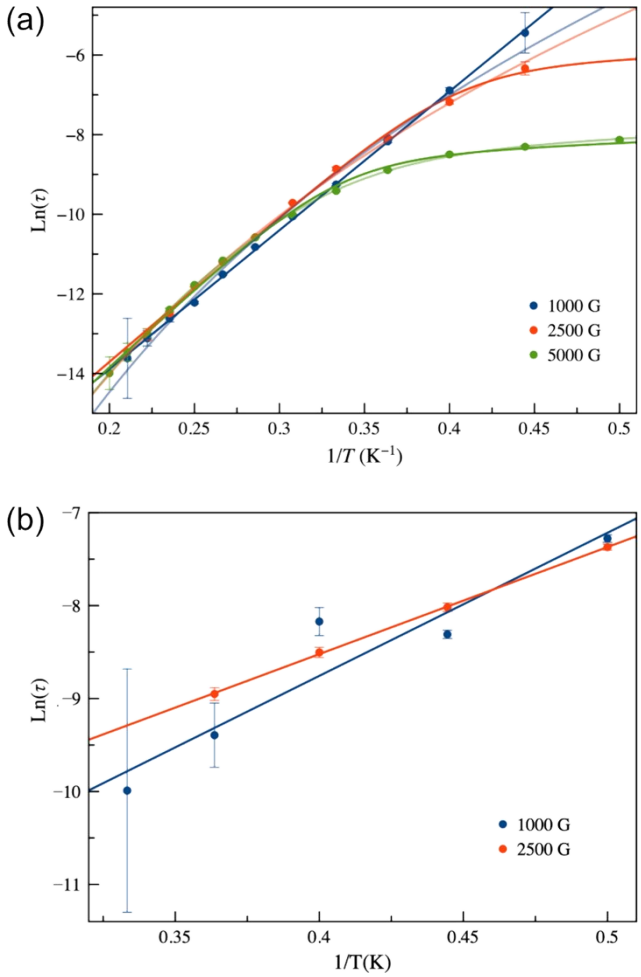

Fig. S16. Arrhenius plots for (a) high- and (b) low-temperature relaxation processes of **2** obtained from individual selection of data in each temperature region. Best fit are shown as solid lines and correspond to combinations of a one-phonon direct [only for (a)] with one thermally activated Orbach (dark colours) or a two-phonon Raman (pale colours) processes under a applied dc fields of 1000, 2500 and 5000 G (a) and 1000 and 2500 G (b). Vertical error bars denote standard deviations.